Ceramics International 47 (2021) 17471–17475

Contents lists available at ScienceDirect

Ceramics International

journal homepage: www.elsevier.com/locate/ceramint

Nano-laminated Ti_3SiC_2 synthesized by cost-effective semi-melting process

Byeong Geun Kim [a], Changwan Nou [b], Sang Hyun Bae [b], Soon-Mok Choi [b,*]

[a] Research Development Division, Gyeongbuk Institute of IT Convergence Industry Technology, Gyeongsan-si, 38463, South Korea
[b] School of Energy Materials Chemical Engineering, Korea University of Technology and Education, Cheonan-si, 31253, South Korea

ARTICLE INFO

Keywords:
MAX phase
Ti_3SiC_2
Carbide
Arc melting
Semi-melting
Cost-effective process

ABSTRACT

Titanium silicon carbide (Ti_3SiC_2) with unique nano-laminated structures was successfully synthesized using an arc melting process with composite pellets of individual elements (Ti, Si, and C). The arc melting process was repeated and process parameters were controlled to form homogeneous high-purity Ti_3SiC_2 phases. In contrast with conventional arc melting, Ti_3SiC_2 phases were prepared by the semi-melting of source pellets, which maintained almost their original forms. This semi-melting process is industrially worthwhile, to keep costs down, because additional manufacturing processes are unnecessary or minimized. The distribution and size of pores and density in the products were controlled by varying the experimental parameters, and the temperature-dependent electrical properties of Ti_3SiC_2-MAX phases were investigated also.

1. Introduction

Ternary carbides and nitrides have a layered structure like graphene, and have the unique characteristics of metals and ceramics. They are represented by $M_{n+1}AX_n$ (N = 1, 2, or 3) as carbide or nitride, so called 'MAX' phases. In the general formula, 'M' represents an early transition metal, 'A' represents a group 13–16 element, and 'X' represents C or N [1–3]. They have excellent electrical conductivity and thermal conductivity like metals, and have high durability and high mechanical strength like ceramics [1–3]. In particular, MAX phases have excellent oxidation resistance and are promising candidates for refractory materials in extreme environments [3].

Ti_3SiC_2 is the most representative material among MAX phases. Many research groups have been tried to synthesize the Ti_3SiC_2 material using various manufacturing processes over the years. Goto and Hirai synthesized Ti_3SiC_2 plates using chemical vapor deposition (CVD) with $SiCl_3$, TiCl, CCl and H_2 gases at 1573 K [4]. Yongming et al. synthesized Ti_3SiC_2 polycrystals by hot-pressing the elemental powders at 1600 for 2 h [5]. The composition of sources was used with non-stoichiometry (3Ti:1.2Si:2C) to avoid the formation of TiC by the evaporation of Si during the high temperature process [6]. Gao et al. prepared dense polycrystalline Ti_3SiC_2 using reactive hot-isostatic pressing [1]. Pourebrahim et al. fabricated high-purity Ti_3SiC_2 using spark plasma sintering with Al addition at 1150 °C [7]. Xu et al. prepared single-phase Ti_3SiC_2 by conventional sintering using tube furnace at 1400 °C [8]. Most of the processes required high temperature and long working times due to the carbides's high melting point, above 2000 °C.

Recently, Abu et al. reported the synthesis of high purity Ti_3SiC_2 using an arc melter with elemental powders [9].

The arc melter is an electric furnace that flows current into the sample and melts with its resistance heat. It is widely used to prepare alloys with various elementals such as steel, transition and rare earth alloys [10]. A schematic diagram of an arc melter is shown in Fig. 1(a). To prevent the oxidation of samples, the entire process is performed in a vacuum with Ar gas atmosphere. The water flows in a copper crucible and the molten sample is slowly cooled to room temperature after processing. The biggest advantage of an arc melter is its shorter process time. In case of a sintering process, it took a long time to prepare homogeneous alloys. For example, more than 3 h is required to reach 1, 000 °C if the heating rate is 5 °C/min. This is also why electric arc furnaces are extensively used in various fields such as the fabrication and re-melting of steel and titanium alloys in industry. However, few studies have been hardly reported on the preparation of MAX phases using an arc melter.

Hence, in this paper, we prepared bulk Ti_3SiC_2 using semi-melting not full melting, of the individual elements (Ti, Si, and C). Interestingly, our samples were incompletely melted in contrast with conventional arc melting. High purity Ti_3SiC_2 was fabricated and its shape was nearly maintained. Its microstructural, morphological, and mechanical properties were investigated.

* Corresponding author.
E-mail address: smchoi@koreatech.ac.kr (S.-M. Choi).

https://doi.org/10.1016/j.ceramint.2021.03.064
Received 7 July 2020; Received in revised form 2 March 2021; Accepted 7 March 2021
Available online 10 March 2021

2. Experimental

Raw materials, Ti (<45um, 99.98%), Si (325 mesh, 99%), and graphite (325 mesh, 99.9995%) were measured by molar ratio with an Si-excess stoichiometric ratio (3:1.2:2) [1]. They were put at a zirconia jar with eight zirconia balls and mixed at 300 RPM for 1 h using a planetary ball mill (Fritsch, Germany). The mixed materials were transferred into a stainless mold (Φ 10 mm x height 11 mm), and compressed to fabricate pellets at 20 MPa using a hand-press (Riken Seiki, Japan).

The as-prepared pellets were placed in a copper crucible in the vacuum chamber of an arc melter (Y&I Tech, Korea) (Fig. 1(b)). When high electric power is input, an arc discharge occurs the gap between the tungsten electrode and pellet. This generates high resistance heat in the pellets, and they are fully melted. In this study, the gap was controlled between 5 and 18 mm. The base pressure was adjusted to 5.0 x 10^{-5} Torr using a rotary pump. Ar gas (99.999%) was input into the chamber and the working pressure was controlled at 350 Torr. About 1020 W and 1670 W electric power was applied. The melting times were 10, 80, and 120 s.

After the first process, the pellets were turned over and arc melting was repeated with the same conditions from one to four times (Fig. 1(c)). The samples were named "*TSC-L or H melting time (#number of repetitive process)*". L and H involve low (1020 W) and high (1670 W) powers, respectively. For example, TSC-L10(#4) means that the arc melting was conducted for 10 s and repeated with four processes at the arc power of 1020 W. The microstructural, morphological and composition analysis of the samples were conducted using X-ray diffraction (XRD, Panalytical B.V, Netherlands) and scanning electron microscope (SEM, JEOL, Japan) equipped with energy dispersive spectroscopy (EDS), respectively. The electric conductivities of the samples were determined by temperature differential and four-probe methods using commercial equipment (RZ2000li, Ozawa Science Co., Japan) under an Ar atmosphere in the temperature range from room temperature to about 590 °C.

3. Results and discussion

At first, the experiments were performed when the arc power was fixed at 1020 W. The distance (arc length) between the tungsten electrode and pellets was 5 mm, and the repetition number of process is once. The results of the products are shown in Fig. 2. The inner images in Fig. 2(a) were TSC-L80(#1) before and after cutting. This shows that the shape of the product was distorted and many pores with various size were formed, which was similar to the results of a previous report [9]. Moreover, unwanted structures (fibers) were found in the inner part of the samples (Fig. 2(b) and (c)). EDS mapping results indicated that they were composed of C (78.37~80.52 at. %) and O (19.41~21.56 at. %) elements and trace (Si: 0.02~0.03 at.%, Ti: 0.04~0.05 at.%)(Fig. 2(d) and (e)).

Fig. 3 shows the XRD patterns of (a) TSC-L80(#1) and (b) TSC-L120 (#1). TSC, TS12, TS53, and TC are the Ti_3SiC_2, $TiSi_2$, Ti_5Si_3, and TiC_x, respectively. Ti_3SiC_2 was mainly formed and secondary phases (TiC_x, $TiSi_2$, and Ti_5Si_3) were generated also [11–13]. In addition, no peaks of fibers were found. We assumed two reasons for this phenomenon; 1) the fibers were amorphous or 2) not detected from XRD beam because of their small quantities in samples. In particular, they were mostly found in the middle and bottom of the samples. This clearly indicates that heat was non-uniformly transferred to all parts of the pellets. The formation of unwanted fibers is an interesting phenomenon, however, this hinders the fabrication of high-quality of MAX phases. The additional study (especially, growth mechanism) on the fibers will be conducted in the future.

Accordingly, we changed the process parameters to optimize the fabrication process as follows: the repetition of the process (from one to four times) and increased the distance between the tungsten electrode and pellets (from 5 mm to 18 mm). In addition, the arc power was changed to about 1670 W. The morphologies of the interior (Fig. 4(a)-4(d)) and surface (Fig. 4(e)-4(f)) of the samples were observed by SEM. First, they were checked to determine the uniform formation of MAX phases, by varying positions (top, middle, and bottom). Nano-laminated structures were clearly found everywhere in the samples (Fig. 4(a)-4(d)). They were well arranged, and pores were partially observed. No unwanted products, such as fibers, were found. These morphological

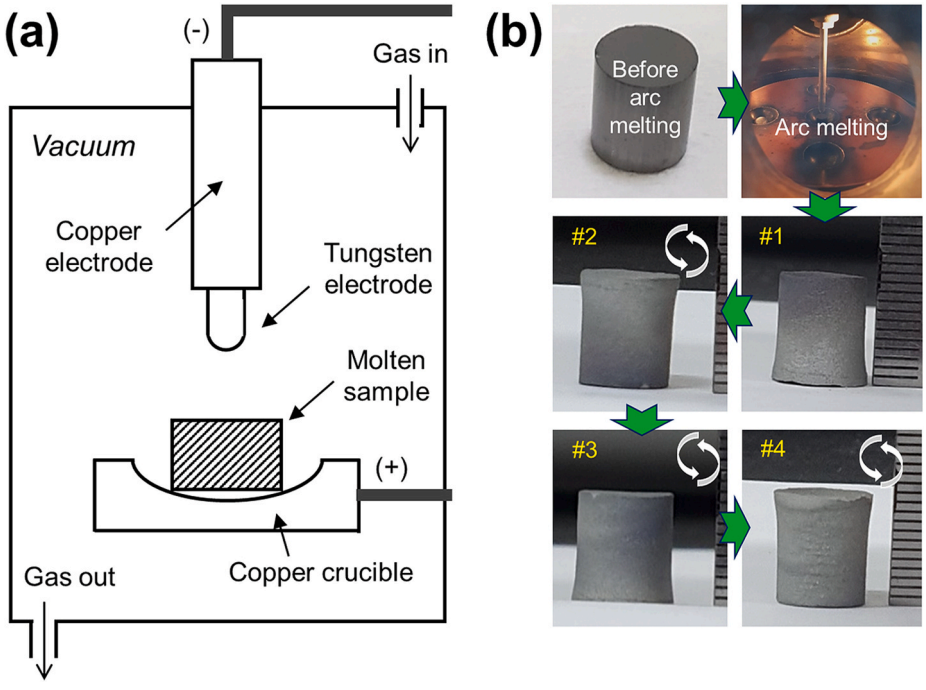

Fig. 1. (a) Schematic of an arc melter and (b) photographs of all processes for preparing samples.

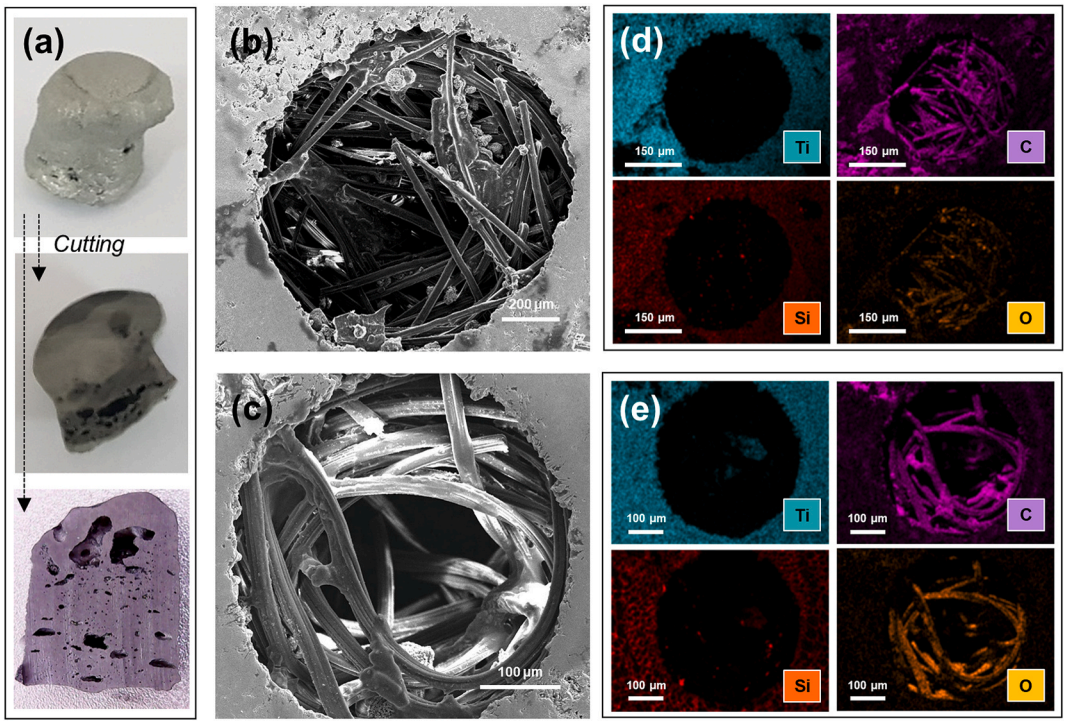

Fig. 2. (a) Photographs TSC-L80(#1), SEM images of (b) TSC-L80(#1) and (c) TSC-L120(#1), EDS mapping images of (d) TSC-L80(#1) and (e) TSC-L120(#1).

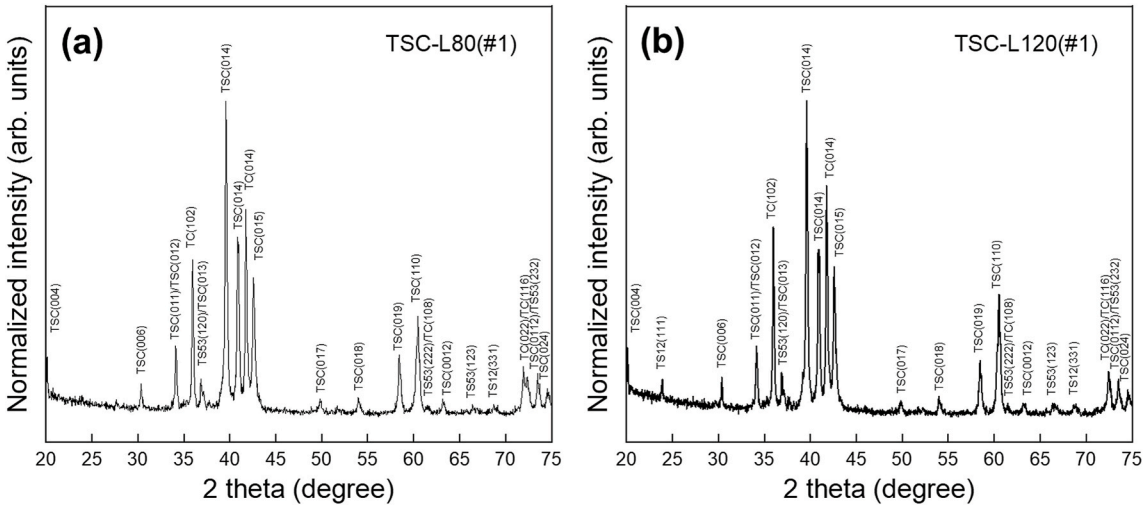

Fig. 3. XRD patterns of (a) TSC-L80(#1) and (b) TSC-L120(#1).

characteristics were also observed in other samples (TSC-H10(#4) and TSC-H80(#80)).

The inner SEM image (yellow arrow in Fig. 4(d)) clearly identified kink bands and delamination of the TSC-H80(#4). The kink structure is one of the unique morphological characteristics of MAX phases [1]. In addition, the SEM image (green arrow) in Fig. 4(d) shows the step meandering and step-flow growth of Ti_3SiC_2 crystals.

The surface morphologies were different than the interior parts (Fig. 4(e)-4(f)). Unlike the inner parts, stacked plates with thicknesses of about 1~2 μm were observed due to the formation of oxides. The 'A' element is oxidized with relative ease, and 'A' oxide is formed [14–16]. It is known that this acts as a healing effect when defects such as crack are formed by external forces [15,16].

Fig. 5(a) shows the XRD patterns of TSC -10(#1), TSC-80(#1) and TSC-120(#1). Sato et al. synthesized Ti_3SiC_2 from a mixture of elemental powders using reaction sintering at 1673K [17], and proposed the reaction mechanism of Ti_3SiC_2 based on the XRD spectra obtained as a function of sintering temperature as follows:

$$Ti + C \rightarrow TiC \quad (1)$$

$$Ti + Si \rightarrow Ti\text{–}Si(l) \quad (2)$$

$$TiC + Ti\text{–}Si(l) \rightarrow Ti_3SiC_2 \quad (3)$$

When the number of repeated arc meltings was increased from one to four times, the peaks of secondary phases (Ti_5Si_3, $TiSi_2$, and graphite phases) remarkably disappeared from the XRD spectra (block arrows in Fig. 5(b)). C is the graphite phases. Moreover, the intensities of the TiC_x phase visibly decreased. When arc melting was repeated, the Ti_5Si_3 and $TiSi_2$ phases were exhausted to form Ti_3SiC_2 as shown in Eq. (3) after reacting with graphite [16] and TiC_x (Eq. (3) and Eq. (4)).

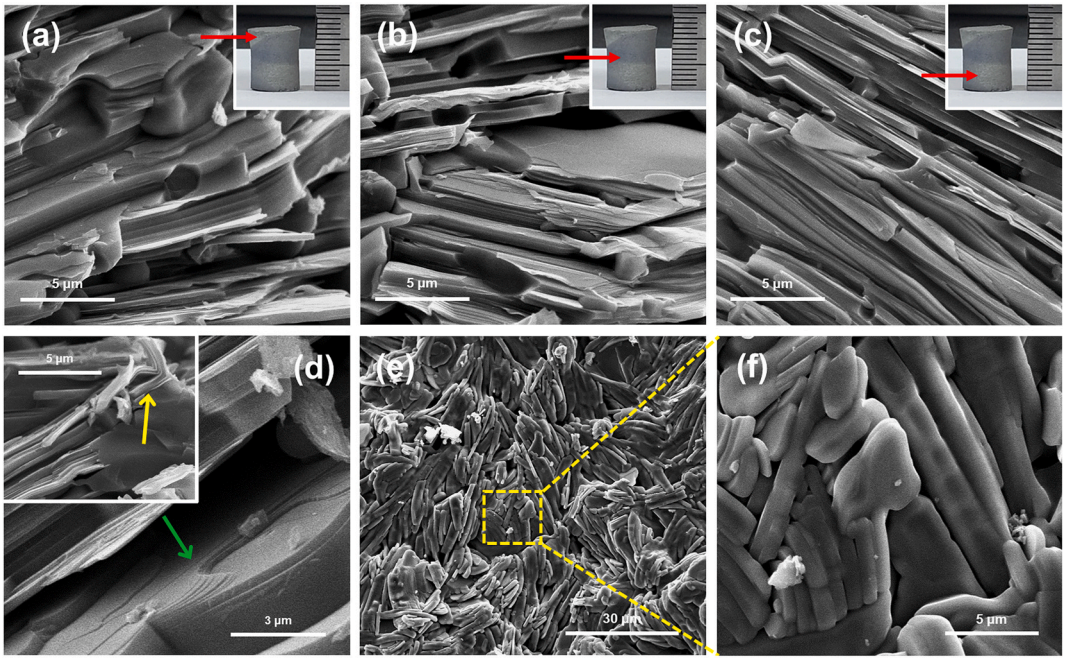

Fig. 4. SEM images of (a)–(c) TSC-H120(#4), (d) TSC-H80(#4), and (e)–(f) TSC-H10(#4).

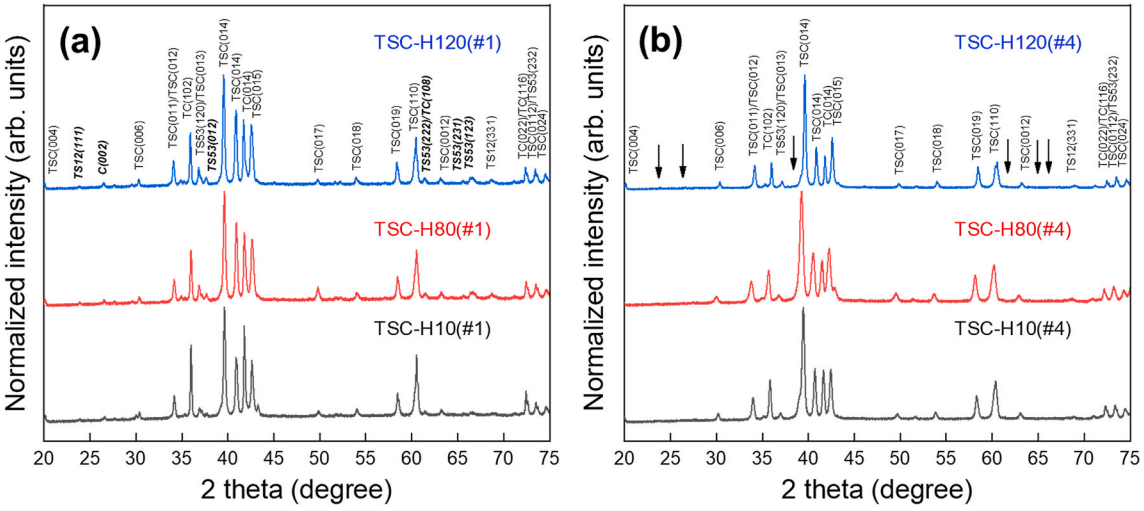

Fig. 5. XRD patterns of the TSC-H10, TSC-H80, and TSC-H120 samples with different numbers of processes: (a) one and (b) four times.

$$C + Ti\text{–}Si(l) \rightarrow Ti_3SiC_2 \quad (4)$$

Fig. 6(a) presents a photograph of TSC-H10(#3). It confirms that many pores (yellow arrows in Fig. 6(a)) were formed on the surface of TSC-H10(#3), and disappeared from the surface of TSC-H10(#4) after arc melting (Fig. 6(b)). The same was true of TSC-H80(#4) and TSC-H120(#4). The formation of pores may originate from the evaporation of Si-related species with low melting point, after the inter-reaction between the Ti, Si, and C sources during the process.

In general, the original shape of the raw materials (pellets) changed when they were wholly melted. Compared with the previous results of another group [9], our samples overall maintained their shape (Figs. 1(b) and 6(b)-6(d)). Hence, we assumed that the products were semi-melted and formed MAX phases. The diameter of the upper part on the pellets was reduced by about 10% after the first arc-melting, while the lower part was not changed (Fig. 1(b)). This indicates that the arc heat was concentrated on the upper part during process #1. The shape of the samples did not change up until process #4. The semi-melting process can reduce cost and time when manufacturing products because the additional machining steps are unnecessary or minimized, indicating that the process is industrially worthwhile.

To further investigate the morphologies of the products, their cross-sections were observed (inner images of Fig. 6(e)). Both pores and cracks were found in the cross-section of TSC-H10(#4), which corresponds with the photographs in Fig. 6(a) and (b). In particular, most pores existed in the upper part. This was due to the abrupt melting and cooling in a short time. When the melting time was increased, the pores were uniformly distributed and their average size decreased: 0.192 mm (TSC-H10(#4)), 0.119 mm (TSC-H80(#4)), and 0.100 um (TSC-H120(#4)). These experimental results present that the distribution and size of pores and density in the products were controlled. The temperature-dependent electric conductivities of samples were investigated and arc listed in Fig. 6(f). Their values were similar to each other. The electric conductivities at room temperature were 2.225 x 10^6 (TSC-H10(#4)),

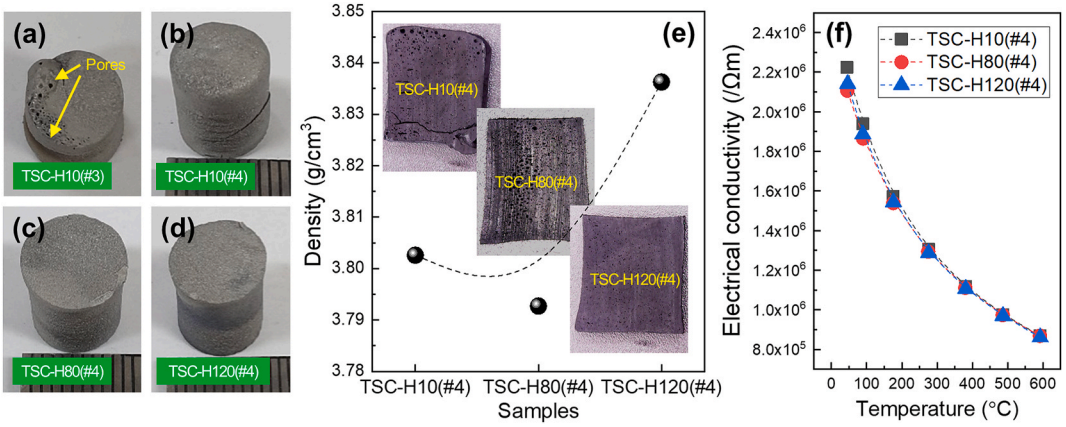

Fig. 6. Photographs of samples: (a) TSC-H10(#3), (b) TSC-H10(#4), (c) TSC-H80(#4) and (d) TSC-H120(#4). (e) Density and cross-sectional images of samples cut vertically from TSC-H10(#4), TSC-H80(#4) and TSC-H120(#4). (f) Electrical conductivities of samples as a function of temperatures.

2.106 x 10^6 (TSC-H80(#4)), and 2.142 x 10^6 (TSC-H120(#4)) (/Ω·m). It gradually decreased with an increase in temperature, and their electric conductivities were 8.690 x 10^6 (TSC-H10(#4)), 8.679 x 10^6 (TSC-H10 (#4)), and 8.608 x 10^6 (TSC-H10(#4)) (/Ω·m) at about 600 °C. This shows that the electric behavior of the samples showed a typical metallic nature [1,7].

4. Conclusion

The Ti_3SiC_2-MAX phase, which maintained its original shape, was successfully fabricated by arc-melting process. Pellets mixed with elemental sources were transformed into the Ti_3SiC_2-MAX phase by the arc melting process, the repeating the process induced the formation of high-quality TSC by removing secondary phases and preventing unwanted products. Controlling the gap between the pellets and tungsten electrode in the arc melter facilitated the acquisition of the Ti_3SiC_2-MAX phase in its original form, due to semi-melting. Control of density and pore size was possible by increasing melting time. The temperature-dependent electrical conductivities of the Ti_3SiC_2-MAX phase were about 2.1 ~ 2.2 x 10^{-6} (/Ω·m) and about 0.8 x 10^{-6} (/Ω·m) at room-temperature and 600 °C, respectively.

Declaration of competing interest

The authors declare that they have no known competing financial interests or personal relationships that could have appeared to influence the work reported in this paper.

Acknowledgments

This research was supported by Basic Science Research Program through the National Research Foundation of Korea (NRF) funded by the Ministry of Education (No. NRF-2018R1D1A1A02086218). This research was also supported by the Basic Science Research Program (No. NRF-2017R1D1A1A09000570). S.-M. Choi thanks the Cooperative Equipment Center at KOREATECH for assistance with SEM and XRD analysis.

References

[1] M. Radovic, M.W. Barsoum, MAX phases: bridging the gap between metals and ceramics, Am. Ceram. Soc. Bull. 92 (2013) 20–27.
[2] M.W. Barsoum, M. Radovic, Elastic and mechanical properties of the MAX phases, Annu. Rev. Mater. Res. 41 (2011) 195–227.
[3] M.W. Barsoum, T. El-Raghy, The MAX phases: unique new carbide and nitride materials, Am. Sci. 89 (2001) 334–343.
[4] T. Goto, T. Hirai, Chemically vapor deposited Ti_3SiC_2, Mater. Res. Bull. 22 (1987) 1195–1201.
[5] L. Yongming, P. Wei, L. Shuqin, C. Jian, W. Rauigang, Jianqiang Li, Synthesis of high-purity Ti_3SiC_2 polycrystals by hot-pressing of the elemental powders, Mater. Lett. 52 (2002) 245–247.
[6] S.-B. Li, H.-X. Zhai, Y. Zhou, Z.-L. Zhang, Synthesis of Ti_3SiC_2 powders by mechanically activated sintering of elemental powders of Ti, Si and C, Mater. Sci. Eng. A. 407 (2005) 315–321.
[7] N.F. Gao, Y. Miyamoto, D. Zhang, Dense Ti_3SiC_2 prepared by reactive HIP, J. Mater. Sci. 34 (1999) 4385–4392.
[8] B. Xua, Q. Chen, X. Li, C. Meng, H. Zhang, M. Xu, J. Li, Z. Wang, C. Deng, Synthesis of single-phase Ti_3SiC_2 from coarse elemental powders and the effects of excess Al, Ceram. Int. 45 (2019) 948–953.
[9] M.J. Abu, J.J. Mohamed, Z.A. Ahmad, Synthesis of high purity titanium silicon carbide from elemental powders using arc melting method, Int. J. Refract. Met. H. 47 (2014) 86–92.
[10] S. Arajs, G.P. Wray, A laboratory arc melter, J. Phys. E Sci. Instrum. 2 (1969) 518–520.
[11] S.B. Li, J.X. Xie, L.T. Zhang, L.F. Cheng, Synthesis and some properties of Ti_3SiC_2 by hot pressing of titanium, silicon, and carbon powders Part 1 – effect of starting composition on formation of Ti_3SiC_2 and observation of Ti_3SiC_2 crystal morphology, Mater. Sci. Technol. 19 (2003) 1442–1446.
[12] S. Yang, Z.-M. Sun, H. Hashimoto, Formation of Ti_3SiC_2 from Ti-Si-TiC powders by pulse discharge sintering (PDS) technique, Mater. Res. Innovat. 7 (2003) 225–230.
[13] B.Y. Liang, Combustion synthesis of Ti_3SiC_2 induced by spark plasma sintering, Mater. Res. Innovat. 17 (2013) 448–452.
[14] D.J. Tallman, B. Anasori, M.W. Barsoum, A critical review of the oxidation of Ti_2AlC, Ti_3AlC_2 and Cr_2AlC in air, Mater. Res. Lett. 1 (2013) 115–125.
[15] W. Zhai, W. Lu, P. Zhang, J. Wang, X. Liu, L. Zhou, Wear-triggered self-healing behavior on the surface of nanocrystalline nickel aluminum bronze/Ti_3SiC_2 composites, Appl. Surf. Sci. 436 (2018) 1038–1049.
[16] G.M. Song, Y.T. Pei, W.G. Sloof, S.B. Li, J.ThM. De Hossonb, S. van der Zwaag, Oxidation-induced crack healing in Ti_3AlC_2 ceramics, Scripta Mater. 58 (2008) 13–16.
[17] F. Sato, J.-F. Li, R. Watanabe, Reaction synthesis of Ti_3SiC_2 from mixture of elemental powders, Mater. Trans. 41 (2000) 605–608.